Journal Pre-proofs

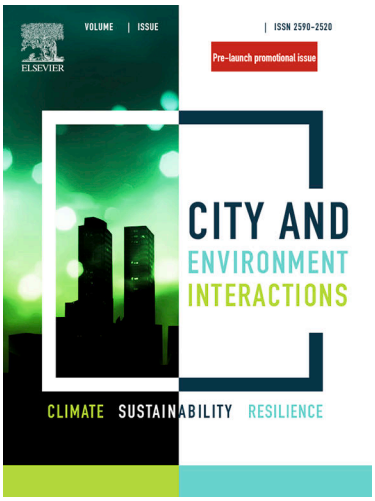

GIS-based revision of a WUDAPT Local Climate Zones map of Bern, Switzerland

Noémie Wellinger, Moritz Gubler, Flurina Müller, Stefan Brönnimann

PII: S2590-2520(23)00037-5
DOI: https://doi.org/10.1016/j.cacint.2023.100135
Reference: CACINT 100135

To appear in: *City and Environment Interactions*

Received Date: 11 September 2023
Revised Date: 11 December 2023
Accepted Date: 13 December 2023

Please cite this article as: N. Wellinger, M. Gubler, F. Müller, S. Brönnimann, GIS-based revision of a WUDAPT Local Climate Zones map of Bern, Switzerland, *City and Environment Interactions* (2023), doi: https://doi.org/10.1016/j.cacint.2023.100135

GIS-based revision of a WUDAPT Local Climate Zones map of Bern, Switzerland

Noémie Wellinger[a,d,*], Moritz Gubler[a,c,d], Flurina Müller[b], Stefan Brönnimann[a,d]

[a] Institute of Geography, University of Bern, Hallerstrasse 12, CH-3012 Bern, Switzerland

[b] School of Agricultural, Forest and Food Sciences HAFL, Bern University of Applied Sciences, Länggasse 85, CH-3052 Zollikofen, Switzerland

[c] Institute for Lower Secondary Education, Bern University of Teacher Education, Fabrikstrasse 8, CH-3012 Bern, Switzerland

[d] Oeschger Center for Climate Change Research, University of Bern, Hochschulstrasse 4, CH-3012 Bern, Switzerland

Abstract

Urban areas are particularly affected by heatwaves through the intensification of heat stress by the urban heat island effect. For effective climate change adaptation, information about microscale surface cover, structures, and human activity in cities is needed to depict the underlying causes of urban heat stress. The framework of "Local Climate Zones" (LZCs) classifies and standardizes urban areas based on such characteristics. To date, most LCZ mapping workflows use satellite imagery as input. The resulting maps may lack some important details, and thus benefit from the use of additional geodata. We introduce a novel approach that combines the geodata of urban canopy parameters with the remote sensing-based LCZ map of Bern, Switzerland. City-specific urban canopy parameters are calculated and used to adjust established value ranges, if necessary. The most common misclassification patterns are identified and misclassified pixels are corrected using a decision tree and k-nearest-neighbor algorithm. Results show that the conformity with the urban canopy parameter values markedly increased, especially in the distinction of water surfaces, non-built areas, and building height. However, for high-resolution LCZ maps, this also leads to unnecessary heterogeneity, which may require further postprocessing. Given sufficiently available urban canopy parameter data, the proposed workflow is simple and easily adaptable for other cities. It could prove useful in urban climate studies and city planning to enhance an existing LCZ map in a contextualized manner quickly.

Key words

LCZ, Urban Heat Island, LCZ Generator, Geodata, Urban Canopy Parameter, Decision Tree

Highlights

- GIS-based workflow to enhance LCZ maps produced with the LCZ-Generator
- Accuracy assessment and revision of the map using urban canopy parameter geodata
- Improved mapping of small-scale structures with a notable impact on local climate
- Straightforward workflow, customizable for other cities

* Corresponding author at: Institute of Geography, University of Bern, Hallerstrasse 12, CH-3012 Bern, Switzerland
Email address: noemie.wellinger@unibe.ch (N.Wellinger)

1 Introduction

Climate change adaptation has become a matter of urgency, particularly in urban areas. High air temperatures are intensified through dense built-up structures, highly sealed surfaces, sparse vegetation, as well as anthropogenic heat emissions. This results in enhanced air temperatures in urban areas compared to their rural surroundings; a phenomenon referred to as the urban heat island (UHI) effect (Oke et al., 2017). UHIs in the urban canopy layer (UCL, layer between urban surface and roof level), are especially pronounced during night due to slow cooling of the urban surface and subsurface (Oke et al., 2017). The UCL is the most relevant layer of the urban atmosphere for human wellbeing (Oke et al., 2017; Stewart & Oke, 2012), which is illustrated by increased risks of morbidity and mortality among vulnerable persons living in urban areas (IPCC, 2023; Oke et al., 2017), causing for example 5.9% excess deaths during the heat summer of 2015 in Switzerland (Vicedo-Cabrera et al., 2016).

Effective climate change adaptation in cities thus requires public health interventions and urban planning acknowledging the causes of UHIs. For modeling or predicting urban heat stress, data about building structure and land cover is essential (Aslam & Rana, 2022a). Aiming for global applicability, Stewart & Oke (2012) introduced the Local Climate Zones (LCZ), as a climatological classification framework for urban areas based on the thermal properties of the local land cover and building type as well as anthropogenic heat fluxes and emissions. Out of the total 17 LCZ classes, 10 refer to specific building types and 7 to the land cover without buildings. They are defined by ranges of 10 urban canopy parameters (UCP). Each LCZ class exhibits a characteristic micro-climatic regime within the UCL "that is most apparent over dry surfaces, on calm, clear nights, and in areas of simple relief" (Stewart & Oke, 2012, p. 1884). LCZs are thus useful for urban climate modeling or for analyses of urban climate measurement data. The horizontal extent of an LCZ can range from a few hundred meters to several kilometers, depending on local conditions. For LCZ classifications, areas of at least one square kilometer are recommended (Stewart and Oke 2012).

Typically, three main methods of LCZ mapping are used: manual, remote sensing (RS), and GIS-based (Quan & Bansal, 2021).

Manual mapping is the most precise but requires extensive time resources and expert knowledge and, thus, is typically not used for city-wide mapping (Stewart & Oke, 2012). It is mostly used to classify single reference sites and to qualitatively evaluate automated LCZ mapping results.

RS-based mapping uses object-based image analysis or supervised pixel-based classification (Gál et al., 2015; Hidalgo et al., 2019). The most used LCZ mapping tool (Aslam & Rana, 2022b) is the LCZ generator, which is based on satellite image analysis and requires solely training areas and metadata as input (Demuzere et al., 2021). The LCZ generator was integrated into the open access "World Urban Database and Access Portal Tools" (WUDAPT) an online database for crowdsourced information about the form and functionality of the UCL worldwide, with LCZ maps being Level 0 data. The LCZ mapping using this framework is therefore further referred to as the WUDAPT L0 workflow (Bechtel et al., 2015). The workflow is globally applicable as satellite images are available for the whole globe. All required software and data are free and the results are publicly available, rendering the LCZ generator easily accessible and well-suited for transdisciplinary applications. On the downside, the machine learning algorithm of the WUDAPT L0 workflow depends on the quantity and quality of the training samples and satellite images (Bechtel et al., 2015 (Mapping LCZ); Ren et al., 2016). Inaccuracies also arise because the building height is difficult to derive from the 2D perspective (Muhammad et al., 2022; Wang et al., 2018). Land cover LCZs are classified more accurately. In mixed-use and heterogeneously built areas, the LCZ generator may struggle to classify the correct dominant LCZ class (Wang et al., 2022; Wicki & Parlow, 2017).

GIS-based mapping approaches use different types of geodata like land cover information, cadastral data, and digital surface models from which UCPs and mapping units are derived. LCZs are then derived using different classification procedures according to the typical UCP value ranges defined by Stewart & Oke (2012). The most commonly used is fuzzy logic to determine the degree of membership to each LCZ (Unger et al., 2014; Gàl et al., 2015, Estacio et al., 2019; Muhammad et al., 2022) Other studies have developed rule-based decision making and clustering algorithms (Geletič & Lehnert, 2016; Hidalgo et al., 2019; Chen et al., 2020). Wicki & Parlow (2017) calculated the UCP values for LULC classes and linked them to the LCZ scheme according to the UCP value ranges defined by Stewart & Oke (2012). Hammerberg et al. (2018) used a probabilistic naïve Bayes classifier. GIS-based LCZ maps generally reach a higher overall accuracy than RS-based maps (Wang et al., 2018; Muhammad et al., 2022).

One major challenge in GIS-based mapping is the global availability of UCP geodata, which varies in quality and quantity, making it challenging to create a globally applicable workflow. One study proposed a method to derive UCPs from Open Street Map data (Fonte et al., 2019). Although LCZs are designed to be globally comparable, they are derived from North American cities' large-scale and homogeneous structures (Wicki & Parlow, 2017) and typically, a minimum LCZ size of 400 m is recommended. Consequently, accuracy issues in GIS-based maps often arise because their LCZs do not match the typical values of UCPs, and small-scale heterogeneous structures cannot accurately be mapped, resulting in mixed pixels (Mitraka et al., 2015; Stewart & Oke, 2012; Wicki & Parlow, 2017). To account for the morphological character of local architectural styles, different studies have

adapted the original UCP value ranges (Geletic et al., 2016; Muhammad et al., 2022), while others mixed, added, or removed som

To overcome some of the shortcomings of RS- and GIS-based mapping and reach higher classification accuracy, combinations of GIS- and RS-based mapping have been suggested (Huang et al., 2023; Quan & Bansal, 2021). Fonte et al. (2019) proposed a weighted combination of GIS-based maps derived from OSM data with fuzzy logic approach and seasonal WUDAPT maps. This allows to weigh the data sources depending on their reliability. Gál et al. (2015) replaced the post-classification majority filtering of the WUDAPT method with an aggregation process used in GIS-mapping, where single pixel LCZs are aggregated to homogeneous zones of at least 250 m. GIS-based approaches are also incorporated into pre-processing by aiding the selection of training data for the WUDAPT workflow. Zhou et al. (2020) extended the WUDAPT L0 workflow by adding a pre-set recognition of the standard LCZ classes to select training areas. By deriving UCPs from building data, DEMs/DSMs, and an NDVI product two sets of training areas were selected, one including the standard LCZ classes by Stewart & Oke (2012), and a second set with additional sub-classes. Muhammad et al. (2022) derived new training areas from a GIS-based mapping approach and used them to improve the WUDAPT mapping result.

There is currently no generally accepted workflow for combined RS- and GIS-based mapping since the research in this field faces, again, multiple challenges such as lacking geodata, unclear methodological specification, and global variability in LCZ properties (Huang et al., 2023; Quan & Bansal, 2021; Stewart & Oke, 2012). The present study thus contributes to the ongoing research on combined LCZ mapping method with a novel approach combining the straightforward and accurate RS-based mapping tool "LCZ generator" with GIS-based LCZ mapping. In detail, we propose an accuracy assessment of the RS-based LCZ map of the city of Bern, Switzerland, using urban canopy parameter (UCP) geodata and a subsequent customized revision of the most dominant patterns of misclassifications, to optimize the accuracy and usability of the LCZ map.

2 Material and Methods

2.1 Study area

The mapped area spans 13.4 km (east-west) by 11.7 km (north-south), covering the entire city of Bern, Switzerland, and parts of the neighboring municipalities. Bern lies at an average elevation of 550 m a.s.l. and has a relatively complex topography affecting the local climate: The surrounding hills alternate with valleys and the Aare River flows through the city in a deeply incised riverbed (Burger et al., 2021; Gubler et al., 2021; Hürzeler et al., 2022). Bern is the fifth largest Swiss city with a population of approximately 135,000, which results in a population density of 2600 inhabitants per km^2 (FSO, 2022). Throughout the reference period of 1991-2020, the official weather station Bern/Zollikofen, located north of the city, registered an annual mean temperature of 9.3 °C and 9.0 heat days on average (maximum temperature ≥ 30 °C). The annual precipitation sums averaged 1022 mm (MeteoSwiss, 2021).

2.2 LCZ mapping and WUDAPT

The 17 standard LCZ classes are grouped into built types (LCZs 1-10) and land cover types (LCZ A-G) (Fig. 1). Each LCZ is characterized by a set of 10 UCPs, which are based on geometric and surface cover properties and allow to compare LCZs independently of construction materials and ambient atmospheric and radiative conditions (Stewart & Oke, 2012; Wicki & Parlow, 2017). These include sky view factor, aspect ratio, building surface fraction, impervious surface fraction, pervious surface fraction, height of roughness elements, and terrain roughness class. Thermal UCPs are surface admittance, surface albedo, and anthropogenic heat output (Stewart & Oke, 2012).

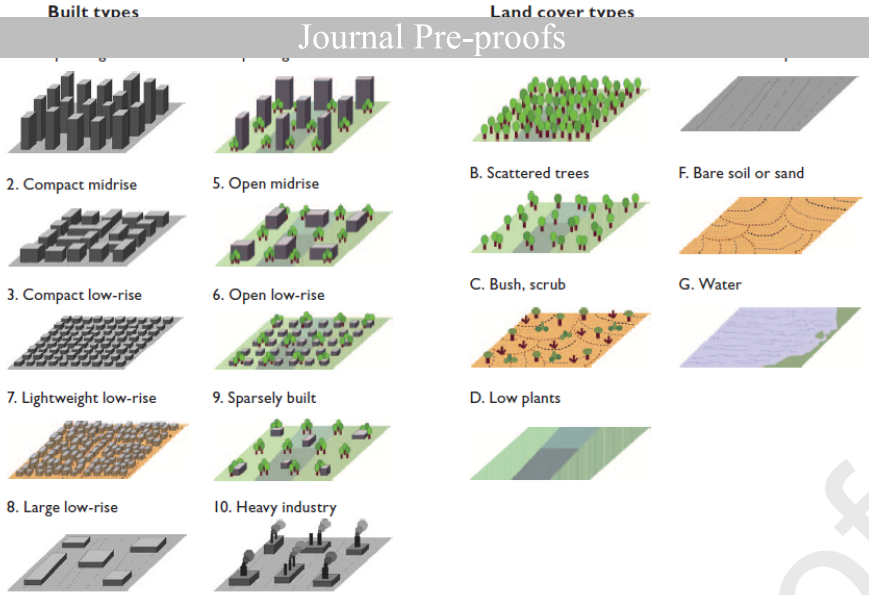

Figure 1: The 17 standard LCZ classes. Source: Stewart and Oke (2012). ©American Meteorological Society. Used with permission.

One way to generate LCZ data is via the open access "World Urban Database and Access Portal Tools" (WUDAPT) which was developed to collect crowdsourced information about the form and functionality of the UCL worldwide. The data can be used to model characteristics of the urban atmosphere and serves as an important basis for urban planning. WUDAPT provides an integrated online tool for generating LCZ maps: the LCZ generator (Demuzere et al., 2021). It provides a variety of earth observation features as input. Its random forest classifier is implemented in Google Earth Engine (Gorelick et al., 2017) to generate LCZ maps using only site metadata and training areas as user input (Demuzere et al., 2021). It replaces the former WUDAPT mapping workflow, which relied on Landsat 8 data (USGS, 2020) as input to a random forest classifier embedded in SAGA GIS (Conrad et al., 2015).

2.3 Data and preprocessing

Even though a minimum pixel size of at least 400 - 1000 m is recommended (Stewart & Oke, 2012) for LCZs, a pixel size of 50 to 100 m was estimated to be more appropriate for an LCZ map of Bern, based on related research about the city's urban climate. Previous studies modelled the temperatures in Bern at a 50 x 50 m spatial resolution using MUKLIMO (Hürzeler et al., 2022) and a LULC regression model (Burger et al., 2021). Their results indicated that Bern has small-scale, heterogeneous structures with a notable warming or cooling effect such as small, vegetated areas and the city's river which is an important source of cold air flows (Burger et al., 2021). These studies used a qualitative LCZ classification of the measurement sites by Gubler et al. (2021) considering their directionally independent microclimate of 100 x 100 m to evaluate the modelling results. An LCZ map of Bern was produced in 2020 using the former WUDAPT L0 workflow in SAGA GIS. This map, further referred to as "WUDAPT map", is the basis for our evaluation and revision using the UCP datasets. Due to unknown reasons, the WUDAPT map was generated at 78.8 x 78.8 m resolution. This resolution was retained, as it was found to be representative of Bern's urban landscape and a resampling to 50 or 100 m may have introduced unidentifiable biases. For further usage, a map in 50 m resolution was resampled from the WUDAPT map and subjected to the same revision workflow (see Appendix). The results of our study, however, exclusively pertain to the revision of the original 78.8 m WUDAPT map.

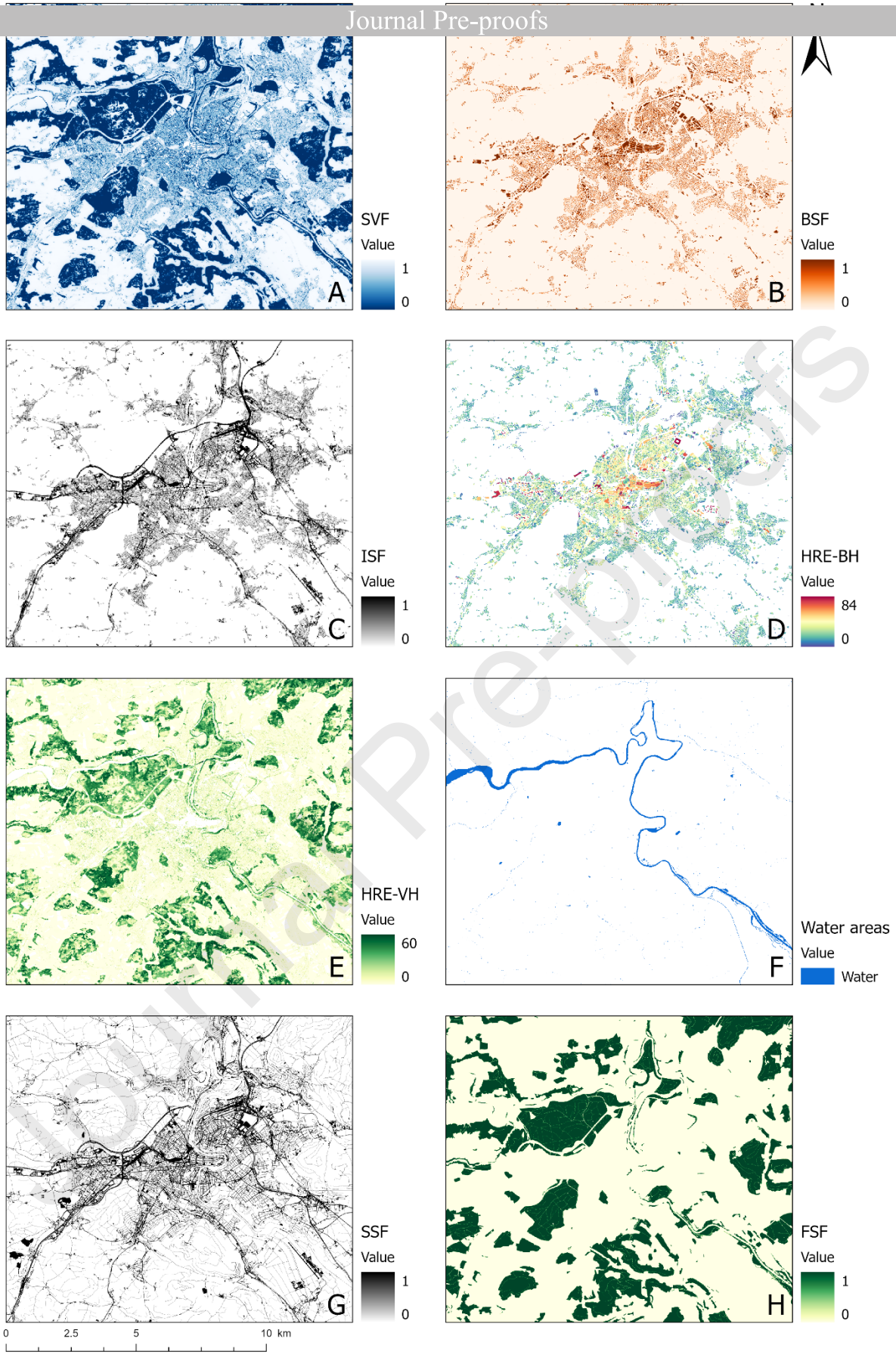

Figure 2: High resolution (10 m pixel size) UCP maps of A) Sky View Factor (SVF) [0 - 1], B) Building Surface Fraction (BSF) [0 - 1], C) Impervious Surface Fraction (ISF) [0 - 1], D) Height of Roughness Elements: Building height (HRE-BH) [m], E) Height of Roughness Elements: Vegetation Height (HRE-VH) [m], F) Water areas [0: no water, 1: water], G) Sealed Surface Fraction (SSF) [0 - 1], and H) Forest Surface Fraction (FSF) [0 - 1]

Table 1: Overview of UCP datasets. SVF, BSF, ISF, and HRE are according to Stewart and Oke (2012). WSF, SSF, and FSF are additional.

UCP		Description	Source	Data type
Sky View Factor	SVF	Ratio of the amount of sky hemisphere visible from ground level to that of an unobstructed hemisphere	Burger et al. (2021)	Raster, 5m
Building Surface Fraction		Ratio of building plan area to total plan area (%)	Burger et al. (2021)	Vector
Impervious Surface Fraction	ISF	Ratio of impervious plan area (artificially sealed soil) to total plan area (%)	European Environment Agency (2020)	Raster, 10m
Height of Roughness Elements	HRE-BH	Arithmetic mean of building heights (BH) (LCZs 1–10) and vegetation heights (VH) (LCZs A–F) (m)	Burger et al. (2021) Ginzler & Hobi (2015)	Vector
	HRE-VH			Raster, 10m
Water Surface Fraction	WSF	Ratio of water body plan area to total plan area (%)	Office for Geoinformation of the Canton of Bern (2021)	Vector
Sealed Surface Fraction	SSF	Ratio of sealed plan area to total plan area (%)	Office for Geoinformation of the Canton of Bern (2021)	Vector
Forest Surface Fraction	FSF	Ratio of forest plan area to total plan area (%)	Office for Geoinformation of the Canton of Bern (2021)	Vector

A total of 7 UCPs are gathered as raster and vector data sets (Tab. 1). Sky view factor (SVF), building surface fraction (BSF), impervious surface fraction (ISF), and height of roughness elements (HRE – either build height (-BH) or vegetation height (-VH)) are adopted from the original framework and obtained from previous research (Burger et al., 2021; Ginzler & Hobi, 2015), the European Environment Agency (2020), and the Office for Geoinformation of the Canton of Bern (2021). As in other studies (Hidalgo et al., 2019; Quan & Bansal, 2021), a few additional surface fraction types are introduced, namely water areas, sealed surface fraction, and forest surface fraction. The latter three were derived from the administrative land cover dataset (Office for Geoinformation of the Canton of Bern, 2021). A few preprocessing steps are performed for specific data sets. Firstly, building footprints are masked in the SVF because the parameter is supposed to be measured at UCL height (1-2 m above ground), and the high SVF values on the rooftops would falsify the data. Secondly, HRE-BH is calculated as the building footprint weighted arithmetic mean of building heights (Quan & Bansal, 2021). Pixels containing no buildings or no vegetation, respectively (for HRE-VH), are masked. Finally, all datasets are converted into raster files on a common 78.8 x 78.8 m grid (Fig. 2).

2.4 Determination and evaluation of city-specific UCP value ranges

Stewart & Oke (2012) established fixed value ranges of UCP-values for each LCZ but noted that "metadata are unlikely to match perfectly with the surface property values [UCP] of one LCZ class" (p. 1891). In this case, the most fitting LCZ class should be determined. Demuzere et al. (2019) conclude from comparing UCP mean values in different LCZ classifications of European cities that some value ranges may need to be redefined. To redefine city-specific UCP value ranges for Bern, the training areas previously defined for the WUDAPT mapping (see Section 2.3) are repurposed. They are polygons covering continuous and homogeneous areas that are representative of the individual LCZ classes in Bern. The mean, the standard deviation, as well as the minimum and maximum value of each UCP are calculated for the training areas of each LCZ class. A confidence interval of +/- 2 standard deviations is defined and compared to the established value ranges, which are adjusted if the confidence interval exceeds them. However, a maximum threshold for these adjustments should be defined. Therefore, based on a sensitivity analysis with 5, 10, 15, and 20% (see Appendix), we decided to make the adjustments conservatively, with no more than 10% (e.g. changing the minimum SVF from 0.3 to 0.2). In few cases, the UCP minima and maxima were set manually. HRE, for example, is not adjusted in every case because the building height is a central factor in distinguishing the LCZ classes. Only the

maximum HRE of LCZs 8-10 are allowed to be adapted. The minimum HRE of LCZ B is reduced from 3 to 2 m, to close the gap to the u[illegible]f different thresholds - from 90% to 70%.

Table 2: Value ranges and means of UCPs used for the revision. Generally, the established value ranges by Stewart & Oke (2012) are adopted, but they are in brackets if new, city-specific values exist for Bern. The mean values of the established value ranges by Stewart & Oke (2012) are listed only for the built type LCZ because they are needed in the further revision process. The italic values are used in our revision algorithm specifically as thresholds to check for misclassified pixels (Tab. 3) and in the subsequent reclassification via decision tree and KNN algorithm (Fig. 4).

LCZ	SVF			BSF			ISF [%]			HRE [m]		
	min	max	*mean*	min	max	*mean*	min	max	*mean*	min	max	*mean*
1	0.19 (0.2)	0.5 (0.4)	*0.35*	0.3 (0.4)	0.7 (0.6)	*0.50*	30 (40)	70 (60)	*50*	25	200	*40.0*
2	0.24 (0.3)	0.7 (0.6)	*0.47*	0.4	0.77 (0.7)	*0.59*	23 (30)	54 (50)	*39*	10	25	*17.5*
4	0.4 (0.5)	0.7	*0.55*	0.1 (0.2)	0.4	*0.25*	20 (30)	50 (40)	*35*	*22 (25)*	200	*40.0*
5	0.4 (0.5)	0.8	*0.60*	0.16 (0.2)	0.44 (0.4)	*0.30*	20 (30)	50	*35*	*10*	*22 (25)*	*16.0*
6	0.5 (0.6)	0.9	*0.70*	0.16 (0.2)	0.4	*0.28*	10 (20)	50	*30*	3	*10*	*6.5*
8	0.6 (0.7)	1	*0.80*	0.2 (0.3)	0.6 (0.5)	*0.40*	30 (40)	60 (50)	*45*	3	20 (10)	*11.5*
9	0.7 (0.8)	1	*0.85*	0.1	0.2	*0.15*	0	28 (20)	*14*	3	20 (10)	*11.5*
10	0.52 (0.6)	0.9		0.2	0.4 (0.3)		20	50 (40)		5	23 (15)	
A	0	*0.4*		0	*0.1*		0	10		3	30	
B	0.42 (0.5)	*0.9 (0.8)*		0	*0.1*		0	10		2 (3)	15	
C	0.6 (0.7)	0.9		0	0.1		0	20 (10)		0	2	
D	0.9	1		0	*0.1*		0	17 (10)		0	*1.6 (1)*	
E	0.8 (0.9)	1		0	*0.1*		*70 (90)*	100				
G	0.8 (0.9)	1		0	*0.1*		0	19 (10)				

Minimum thresholds for the newly defined surface fractions are set only for the relevant LCZ classes. Different thresholds are tested and compared visually before settling on the following: LCZ A is characterized by FSF >=0.8, LCZ E by SSF >= 0.7, and LCZ G by WSF >= 0.4.

LCZ 3 (compact low-rise), 7 (lightweight low-rise), and E (bare soil or sand) do not occur in Bern.

2.5 Qualitative analysis of main misclassifications in the WUDAPT map

Using the city-specific UCP value ranges, an initial statistical accuracy analysis is conducted, providing percentages and distributions indicating value range conformity for each UCP and each LCZ. This, combined with a visual examination of the LCZ map against aerial photos, allows to identify prominent misclassification patterns. Depending on building structure, surface cover, climate zone, input data, and mapping algorithm quality, these patterns may differ from city to city. They guide the subsequent revision steps. Therefore, it is advised to focus on a few commonly occurring patterns, particularly on those that occur in thermally and morphologically very different LCZ classes and would presumably influence the results of numerical models based on LCZs and impair the maps usability in city planning for heat mitigation.

In this paragraph, we present some suggestions on how to select the patterns and how to adapt these rules for other urban morphology types. Generally, confusions between LCZs of similar thermal behavior weigh in less than between thermally different LCZs (Chen et al., 2020). This may be slightly different from city to city (see the Appendix for a brief analysis of thermally similar LCZs in Bern). Confusion between built type and land cover type LCZs will most likely appear in all LCZ maps and can be easily checked using the BSF. This should be the first step, to have a clear grouping of built and non-built pixels. In a very green city, it will also be important to differentiate between compact (1-3) and open built (4-6, 9) LCZs using the BSF, aspect ratio, and UCPs indicating vegetation cover and sealing such as ISF, PSF and VH. In a highly sealed city, the building height and spacing (differentiation of LCZ 1-3, 7, 8, 10) may be more important. For this, BH, SVF and aspect ratio can be used. Building height can be difficult to be recognized by the LCZ generator, and therefore may cause numerous misclassifications (Muhammad et al., 2022; Wang et al., 2018). Single pixels and boarders between LCZs in the WUDAPT map should be examined specifically since they are prone to be misclassified. Vegetated land cover LCZs can be distinguished if there is VH and/or SVF data available. An NDVI product may help to distinguish vegetated areas from non-vegetated areas (Zhou et al., 2020), and, especially in dry climates, bare ground, or dry, non-cooling vegetation from green vegetation. Furthermore, with local knowledge of the city, areas of special interest, measurement stations, small-scale structures, and areas that are known to have a particular heating or cooling effect can be examined on the map in order to see if the WUDAPT workflow classified them correctly. It is advisable to use aerial or satellite images as a reference to visually compare with the LCZ map. If the city is subjected to seasonal climate variations, pictures of different seasons might support the identification of misclassifications. Lastly, removing LCZ classes that don't exist in the area of interest, allows to identify pixels of these classes as misclassifications directly and simplify the revision algorithm. LCZ classes can also be excluded only from the revision, meaning that existing pixels of this class will be left on the map, but no new pixels will be classified in the revision. This can be helpful if there are not enough or no suited UCP geodata available to identify this class, or if the class is very rare to avoid the risk of wrong reclassification of pixels.

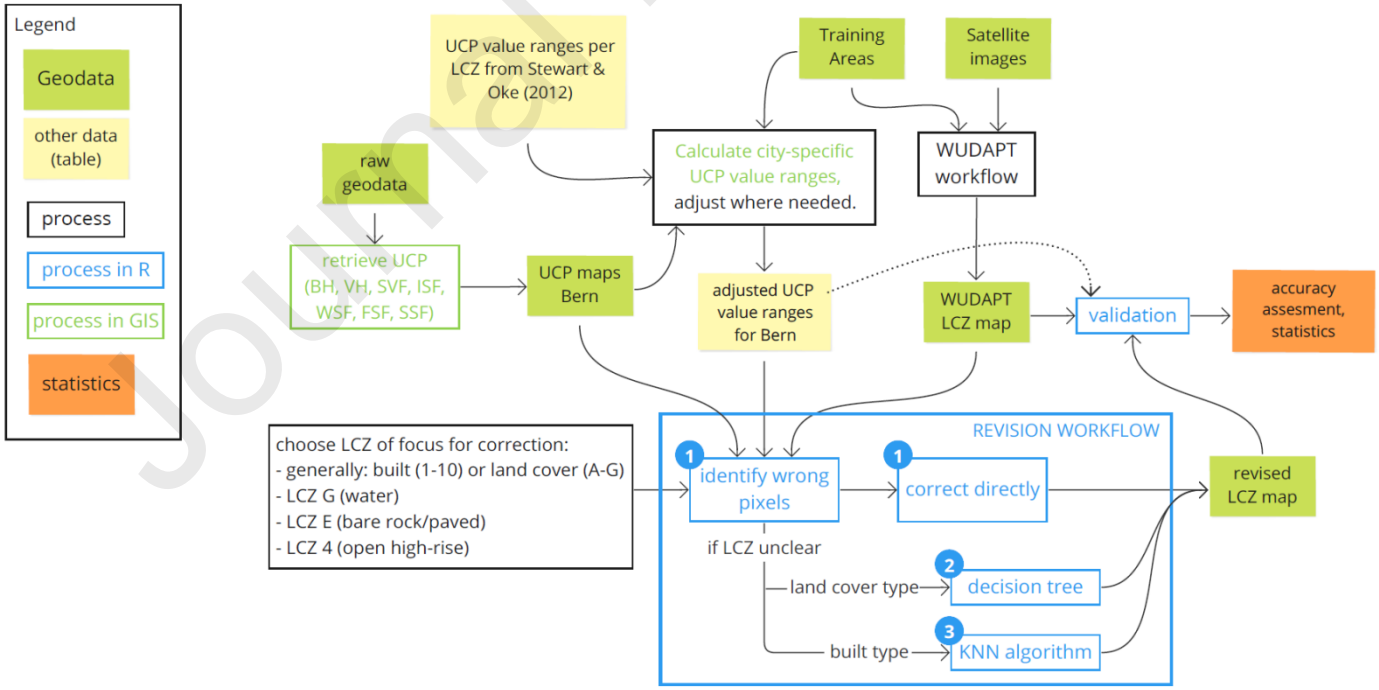

Figure 3: Overview of our workflow. It shows all input data and processing steps from creating a WUDAPT map with the LCZ Generator (Demuzere et al., 2021) *to revising it with our proposed workflow to get the final revised map. All the processing steps (black, blue, or green bordered) are described in detail in Sections 2.2 – 2.6*

2.6 Revision

Table 3: Queries for identifying misclassified pixels (revision step 1, see Fig. 3). This specific order, as listed, is essential because some queries are based on previous ones. The new LCZ is either directly classified or marked as unclear (NA) and passed to revision step 2 (see Fig. 4).

LCZ in WUDAPT map	Query	LCZ in revised map
LCZ 1-10 vs. A-G	`LCZ == 1-10 AND BSF < 0.08`	unclear
	`LCZ == A-G AND BSF > 0.12`	unclear
LCZ G (Water)	`LCZ != G AND WSF >= 0.4`	G
	`LCZ == G AND WSF < 0.4`	unclear
LCZ E (bare rock or paved)	`LCZ != E AND (BSF < 0.1 AND (ISF >= 0.7 OR SSF >= 0.7)`	E
	`LCZ == E AND (BSF >= 0.1 AND (ISF < 0.7 OR SSF < 0.82)`	unclear
LCZ 4 (open high-rise)	`LCZ == 4 AND BSF < 0.08`	unclear
	`LCZ == 4 AND 10 <= BH < 22`	5
	`LCZ == 4 AND BH < 10`	6

The revision of the LCZ map proceeds in three steps (Fig. 3): In step one, misclassified pixe
chosen four selected misclassification patterns (Table 3, see also Sect. 3.1). The queries only check on characteristic variables for the LCZ type, i.e., BSF for the distinction of LCZ 1-10 and LCZ A-G, WSF for LCZ G, BH for LCZ 4, as well as BSF, ISF, and SSF for LCZ E). In some cases, the correct LCZ can immediately be determined; in other cases, the pixel or unit is flagged as unclear, meaning the LCZ must be reclassified in the following steps. In step two (Fig. 3), land cover type LCZs are reclassified via a manually constructed decision tree (Figure 44). The built type LCZs are not unequivocally distinguishable by just one or two UCP values due to frequent overlapping of their UCP value ranges and missing UCPs such as *aspect ratio* and *anthropogenic heat output.* Therefore, a machine learning algorithm is more appropriate to find the most fitting LCZ. Here, a k-nearest-neighbor (KNN) algorithm is applied (James et al., 2013). This classification procedure classifies the remaining unclassified LCZ units based on training data (in this case, 4-dimensional data points from the mean values of the four UCPs from Tab. 2) by identifying the k closest training data points and choosing the most frequently occurring class. Since there is only one training data point per LCZ, k is set to 1. LCZ 10 (heavy industry) is excluded from this process because it shows many similarities to LCZ 8 in Bern, and many pixels were misclassified as LCZ 10 during test runs. The extent of this zone in Switzerland, notably in Bern, is debatable due to the outsourcing of most heavy industry to the outside of the cities and to other countries. Choosing classification features like silos and chimneys results in certain waste incineration, sewage treatment plants, or other industrial sites (LCZ 8) with taller buildings being classified as LCZ 10 by the LCZ generator.

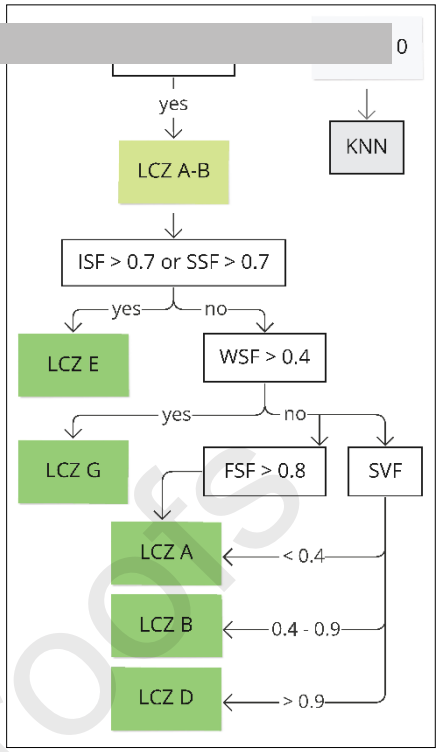

Figure 4: Decision tree. The darker green boxes mark the final LCZ class. Pixels of LCZs 1-10 are passed on to the KNN algorithm (revision step three)

2.7 Evaluations

To evaluate the results of the revision and the usability of the approach, three types of evaluations are conducted. First, a quantitative analysis provides an overview of the reclassification results, highlighting spatial and LCZ class-specific changes. A confusion matrix displays the reclassifications among all LCZ classes and change rates. To analyze which classes are thermally different in Bern, data from the 80 stations of the urban climate measurement network in Bern is used (Gubler et al., 2021). The LCZ of each site is manually classified using satellite imagery and on-site photos. Then, mean nighttime (10PM to 7AM) temperatures of the summer 2023 (June-August) are aggregated from a 10-minute temporal resolution and the distribution of mean temperature per LCZ class is plotted (Appendix: Fig. 2). A Kruskal-Wallis test and a post-hoc Dunn's test for pairwise multiple comparison are performed on the same temperature data. The Dunn's test indicates which LCZ classes are significantly different from each other. These pairs are then marked in the confusion matrix. Second, a visual assessment is performed in two selected areas to emphasize marked changes. Comparing the WUDAPT and revised LCZ maps with aerial photographs allows for a qualitative evaluation of classification accuracy.

Lastly, a statistical evaluation before and after the revision assesses if the UCPs of a pixel conform to the value ranges (both the original ones by Stewart & Oke (2012) and the Bern-specific ones) of the classified LCZ. Pixels conforming to all examined UCP value ranges (SVF, BSF, ISF, HRE, and WSF) are considered correctly classified. The overall accuracy (OA) is defined by the percentage of pixels conforming to all examined UCP value ranges. Improvements of the approach are quantified via the percentual increase of pixels in agreement with the Bern-specific UCP value ranges. Additionally, percentual differences of correctly classified pixels compared to a revision with the original UCP value ranges by (Stewart & Oke, 2012) quantify the influence of the UCP adaptation on the result. HRE is not analyzed for LCZ E and G because the two classes are neither characterized by buildings (HRE-BH) nor vegetation (HRE-VH). Theoretically, they would exhibit values of 0 HRE, but in practice, an LCZ E or G pixel will likely contain some patch of vegetation or building fraction, which influences the HRE, especially when mapping on a pixel basis.

3 Results

3.1 Misclassification patterns in the WUDAPT LCZ map

Our analysis shows that the WUDAPT-based approach represents a majority of LCZs well. In the following, the four main misclassification patterns are described shortly by referring to their influence on the local climate.

For Bern, we identified four main misclassifications, which appear frequently and would presumably influence the results of numerical models based on LCZs and, thus, are worth revising: 1) The correct distinction of built type (LCZ 1-10) and land cover

type LCZ (A-G), 2) Water bodies (LCZ G), 3) bare rock or paved (LCZ E), and 4) open high rise (LCZ 4). Generally, confusions betv

misclassifications can easily be detected algorithmically using building footprints, water surface data, and land cover data.

- Sparsely built LCZs are confused with land cover LCZs, and vice versa. The correct **distinction between built type (1-10) and land cover type LCZs (A-G)** is essential because the two groups differ significantly in form, function, and thermal properties. Built and sealed areas are characterized by reduced airflow and increased turbulence because of the terrain roughness, as well as increased sensible heat fluxes through heat stored in building materials and reduced latent heat fluxes due to the limited water-storing capacities of the surfaces (Oke et al., 2017).
- Water bodies (**LCZ G**) are mapped in a fragmented, sometimes inaccurate way, small water bodies are disregarded, and bright forest surfaces or gravel roads are misclassified as LCZ G. The correct mapping of water bodies (LCZ G) is critical to LCZ mapping because water can have a strong cooling effect. In particular, the river Aare in Bern alters the UHI, and cold airmasses may accumulate in the riverbed (Burger et al., 2021; Gubler et al., 2021).
- Small-scale **LCZ E** (bare rock or paved) are misclassified as built type LCZs or as pervious land cover LCZs. LCZ E differs strongly from other land cover type LCZ and built type LCZ. Due to its high imperviousness, latent heat fluxes are reduced compared to pervious, vegetated areas, and the lack of buildings creates different ventilation situations (Oke et al., 2017).
- **LCZ 4** (open high rise) is overrepresented, meaning the classification algorithm overestimates the building height. Again, building height influences ventilation, radiative properties, and UCPs such as the SVF.

3.2 Quantitative and spatial overview of the reclassifications

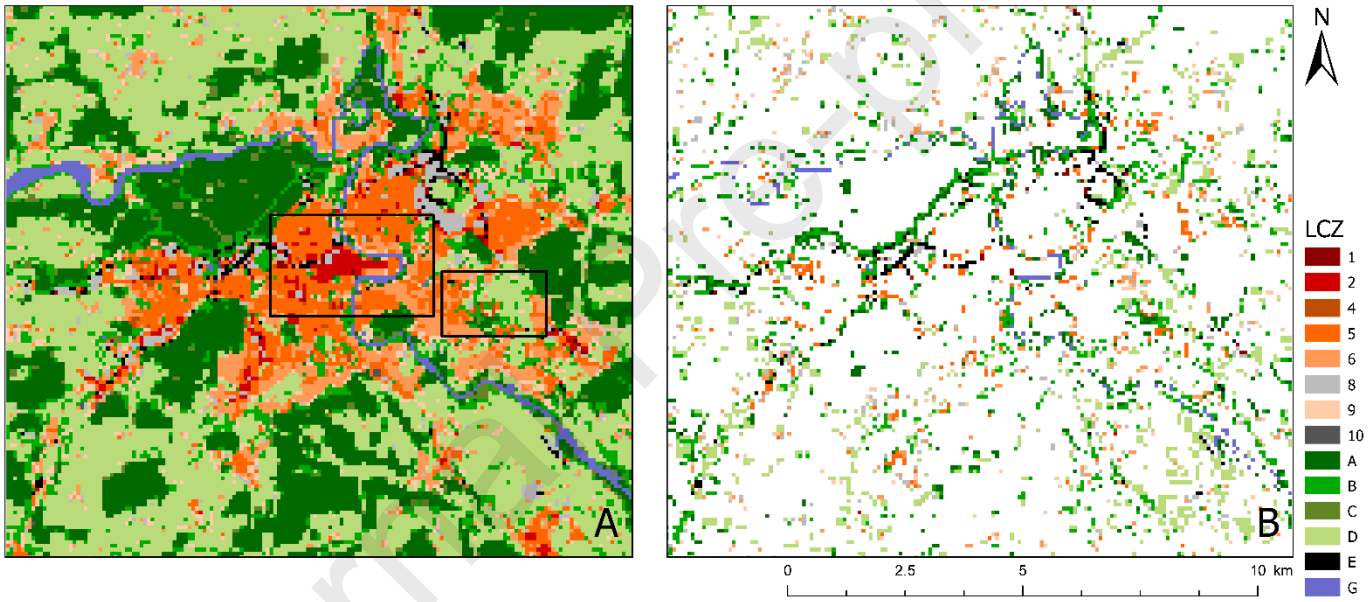

Figure 5: Revised LCZ map with the extents of Figure 6AB and 6CD marked as black rectangles, and B) all pixels changed in the revision process

The final map (Fig. 5A) shows reclassified pixels across the entire area (Fig. 5B). However, they mainly appear along water bodies, i.e., the Aare River, on the borders of built areas, across sealed areas such as highways, and in sparsely built areas in and around the city. A total of 4522 pixels, or circa 18% of the map, were reclassified (Table 4).

Table 4: Confusion matrix of the reclassified pixels among LCZ classes. The horizontal boxes show the revised map, the vertical boxes show the WUD[illegible]type LCZ using the decision tree (top right), reclassifications within land cover type LCZ (bottom right), reclassifications from land cover type to built type LCZ using the KNN algorithm (bottom left), and reclassifications within built type LCZ (top left). Below are the total numbers and ratios of pixels in the respective LCZ class after the revision, as well as the absolute changes, and the percentages of pixels that remained unchanged, i.e., were correctly classified in the WUDAPT approach. The blue cells indicate reclassifications between thermally different LCZ classes.

		LCZ revised																	
		Built type LCZ								Land cover type LCZ									
		1	**2**	**4**	**5**	**6**	**8**	**9**	**10**	**A**	**B**	**C**	**D**	**E**	**G**	total pixels			
LCZ original	built type	**1**																	

LCZ original			1	2	4	5	6	8	9	10	A	B	C	D	E	G	total pixels			
built type	**1**		11	0	0	0	0	0	0	0	1	0	0	0	0	0	12	0.0%		
	2		0	366	0	0	0	0	0	0	1	6	0	14	27	0	414	1.6%		
	4		0	0	94	253	86	0	0	0	46	114	0	26	25	1	645	2.6%		
	5		0	0	0	2171	0	0	0	0	27	132	0	171	41	4	2546	10.1 %		
	6		0	0	0	0	1754	0	0	0	46	138	0	179	20	9	2146	8.5%	9069	36%
	8		0	0	0	0	0	388	0	0	10	30	0	56	67	4	555	2.2%		
	9		0	0	0	0	0	0	790	0	403	627	0	813	6	69	2708	10.8 %		
	10		0	0	0	0	0	0	0	27	4	3	0	2	0	7	43	0.2%		
land cover type	**A**		0	0	0	5	7	4	11	0	5466	0	0	0	0	27	5520	21.9 %		
	B		3	1	5	19	52	44	48	0	0	1245	0	0	2	14	1433	5.7%		
	C		1	0	0	0	4	2	1	0	0	0	335	0	0	21	364	1.4%	16112	64%
	D		4	4	1	45	145	156	138	0	0	0	0	7664	6	7	8170	32.4 %		
	E		15	0	0	1	0	53	0	0	0	8	0	6	20	0	103	0.4%		
	G		0	1	2	3	7	11	8	0	97	58	0	7	0	328	522	2.1%		
total pixels			34	372	102	2497	2055	658	996	27	6101	2361	335	8938	214	491	**25181**			

	0.1%	1.5%	0.4%	9.9%	8.2%	2.6%	4.0%	0.1%	24.2 %	9.4%	1.3%	35.5 %	0.8%	1.9%	
				26.8%							73.2%				
abs. change	22	-42	-543	-49	-91	103	-1712	-16	581	928	-29	768	111	-31	
unchanged	11	366	94	2171	1754	388	790	27	5466	1245	335	7664	20	328	20659
				5601							15058				
	91.7 %	88.4 %	14.6 %	85.3 %	81.7 %	69.9 %	29.2 %	62.8 %	99.0 %	86.9 %	92.0 %	93.8 %	19.4 %	62.8 %	
				61.8%							93.5%				82.0%

A clear systematic of misclassifications, in the sense that "LCZ x is solely misclassified as LCZ y", cannot be determined. However, observable tendencies (Tab. 4) align with the discussed revision focus points (Section 3.1). Pixels are only corrected if they are checked for UCP value conformity in revision step 1 (Fig. 3, Tab. 3). No new pixels are classified as LCZ 10 and C because these classes were excluded from the revision. Changes appear primarily in land cover type LCZs misclassified as built type LCZs (Tab. 4, top right). Reclassifications within built type LCZs (Tab. 4, top left) occur only from LCZ 4 to 5 and 6 due to the design of revision step 1 (Tab. 3). No reclassifications occur among LCZs A, B, C, and D (Tab. 4, bottom right), as these are only corrected if they belong to built type LCZs, or LCZ E, or G. The correct distinction of LCZ E and G is important, as they differ markedly from the other land cover type LCZs. Reclassifications by the KNN algorithm (Tab. 4, bottom left) appear primarily in LCZs B and D, reclassifying them to LCZ 6 and 9 in sparsely built-up or peripheral areas where buildings were "overlooked" by the random forest classification procedure of the WUDAPT workflow. The absolute changes (Tab. 4) indicate a reduction in pixels within built type LCZs, as well as LCZ C and G, after reclassification. The rates of unchanged pixels (Tab. 4), especially in LCZ 4 (14.6%), 9 (29.2%), and E (19.4%) suggest low accuracy in the WUDAPT classification for LCZ 4, 9, and E, while LCZ 1, A, C, and D show high accuracy (>90%). Land cover type LCZs are generally classified more accurately (93.5%) than built type LCZs (61.8%). 691 (2.7%) pixels were changed in thermally significantly different LCZs. With 18% of all pixels reclassified in the course of the revision, this means that 15% of the changes occurred between thermally different classes.

In summary, the reclassifications accurately reflect the four misclassification patterns (Section 3.1). They tend to occur at the edges of built-up zones and in sparsely built-up areas, as well as in LCZs E, G, and 4 (Fig. 5). Thus, the choice of revision foci likely overcame the most severe misclassifications. However, whether these represent general weaknesses of LCZ classifications with WUDAPT or whether additional revision foci would reveal different reclassification patterns remains open.

3.3 Visual evaluation of two representative city areas

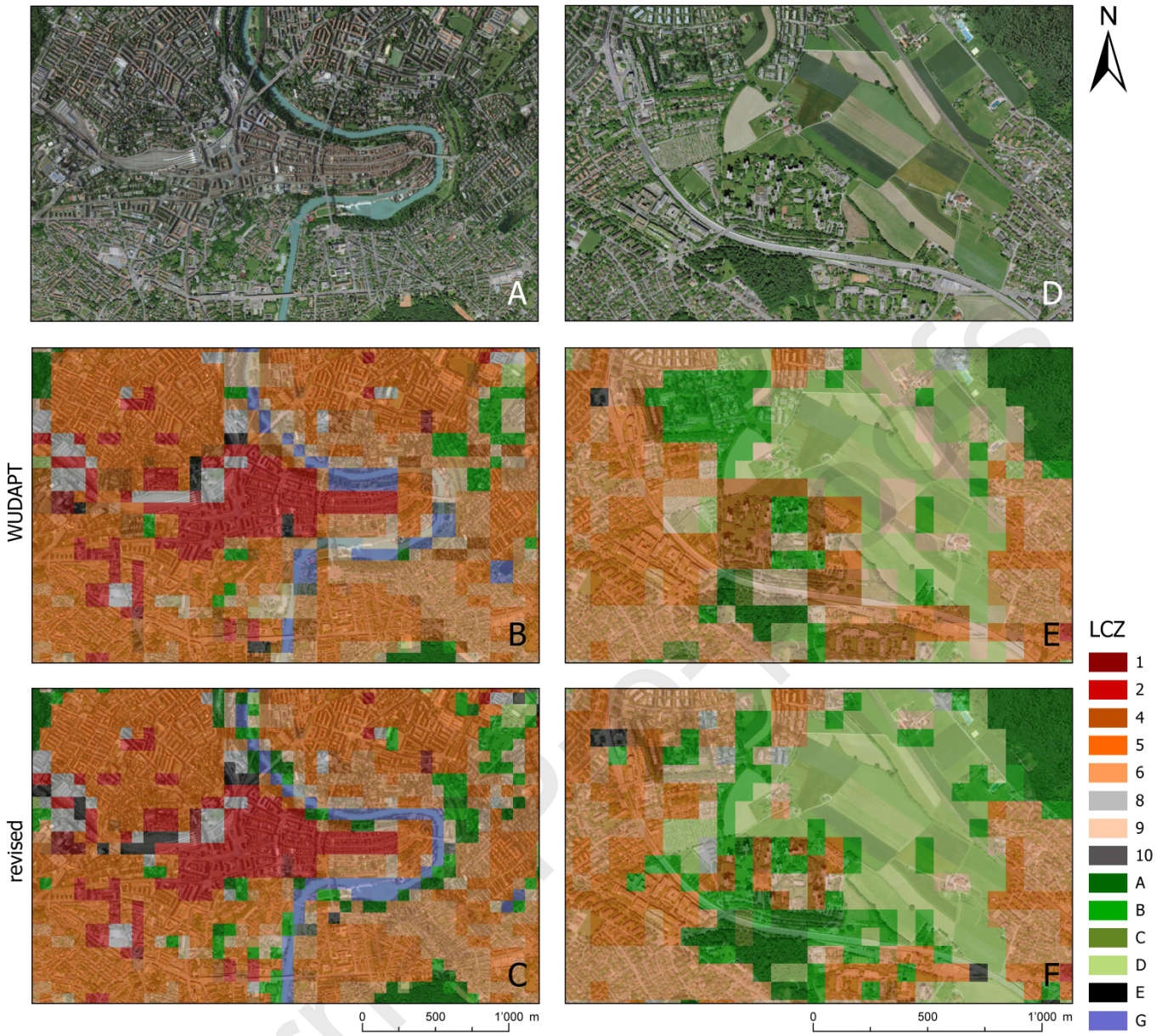

Figure 6: Aerial photos of Bern's city center around the old town (A) and a peripheral area of the city (Schosshalde/Murifeld) (B) are overlayed with the WUDAPT map (B and E) and the revised map (D and F). Aerial photos: swisstopo (2022) © swisstopo

Crosschecking the original and revised LCZ maps with aerial photographs (Fig. 6) allows a qualitative evaluation of the classification accuracy. The following passage evaluates two selected areas within the Bernese municipal area and the most important changes highlighted.

In both areas (Fig. 6C+F), the distinction and borders of built type and land cover type LCZs is more precise after the revision, as each pixel has been checked for BSF. The extent of forest patches, pastures, inner-city parks, and residential areas is displayed accurately. Reclassifications of built type LCZ can primarily be observed in LCZ 4 and 9. Some pixels without high-rise buildings are reclassified from LCZ 4 to LCZ 5 or 6 according to their BH values. Portions of highways are recognized as LCZ E when ISF/SSF values are sufficiently high (Fig. 6BC+F). In the center/old town area (Fig. 6A-C), LCZ G and the green areas along the river are represented more accurately (Fig. 6C). A few cases of newly classified LCZ 9 pixels occur surrounded by compact building areas. In the peripheral area (Fig. 6D-F), extended areas misclassified as LCZ 9 have been reduced to pixels that contain buildings, with 70.8% of the original LCZ 9 pixels reclassified as land cover type LCZs, often LCZ D (Tab. 4). In the center of the map lies the neighborhood "Wittigkofen", correctly identified as LCZ 4 in the WUDAPT map (Fig. 6E). The green areas between buildings are big enough to be reclassified as separate LCZs B, resulting in a checkerboard-like pattern (Fig. 6F). Throughout the whole revised map (Fig. 5A), single pixel LCZ cases can be observed on small, vegetated areas, water bodies, or sealed areas with minimal building fraction, such as highways (Fig. 6F). These and the checkerboard-like patterns are later discussed as "unnecessary

heterogeneity" (see Section 4.2) because it is questionable whether such structures are large enough to be classified as separate
singl

3.4 Statistical evaluation

The agreement with the Bern-specific UCP value ranges increases in the majority of LCZ classes (Fig. 7, Fig. 8). The revised map exhibits an OA of 53%, representing an 9% improvement with respect to the WUDAPT map (Fig. 7). The OA (Fig. 7E) is defined by the percentage of pixels conforming to all examined UCP value ranges (SVF, BSF, ISF, HRE, and WSF; Fig. 7A-D). It should be noted that this is a very strict criterion without buffer, tolerance, or weighting, suggesting that the proportion of correctly classified pixels is likely higher. Also, the OA after a revision with original UCP values ranges by Stewart & Oke (2012) would be 7% lower (at 46%). 91% of all pixels fall within the specified BSF values, whereby the agreement is especially high in land cover LCZ types (Fig. 7C), while built type LCZ tend to have too small BSF values (Fig. 8B). The agreement was already high before the revision, except for LCZ E, which shows an improvement of approximately 67%. LCZ G exhibits very high agreement in BSF (97%), ISF (88%), and WSF (100%). LGZ G's SVF agreement is lower at 30% (Fig. 7), and HRE-VH has values of up to 33 m (Fig. 8D), likely due to factors such as the WSF threshold for classification (0.4) or landscape structures like trees along water banks and the deep riverbed of the Aare River. LCZ E also shows comparatively big improvements, with 70% OA (Fig. 7E, Fig. 8A-C). LCZ 4 achieves 100% compliance within the specified HRE-BH interval, representing an 84% improvement and a 30% difference compared to a revision with the original UCP value ranges, owed to the reduction of the BH threshold from 25 to 22 m (Fig. 7D, Fig. 8D). LCZ 9 shows a notable decrease of 19% in ISF conformity (Fig. 7B), with elevated ISF values (Fig. 8C), likely due to the restriction of LCZ 9 areas to pixels with BSF over 10%.

Figure 7: Comparison of pixel conforming (%) to Bern-specific UCP value ranges after revision (green), before the revision (white), and pixels of the revised map conforming to the original UCP ranges (grey). The Overall Accuracy (OA) measures pixels conforming to all tested UCPs, the groups labelled "all" represents % of pixels of all LCZ classes conforming to the respective UCP

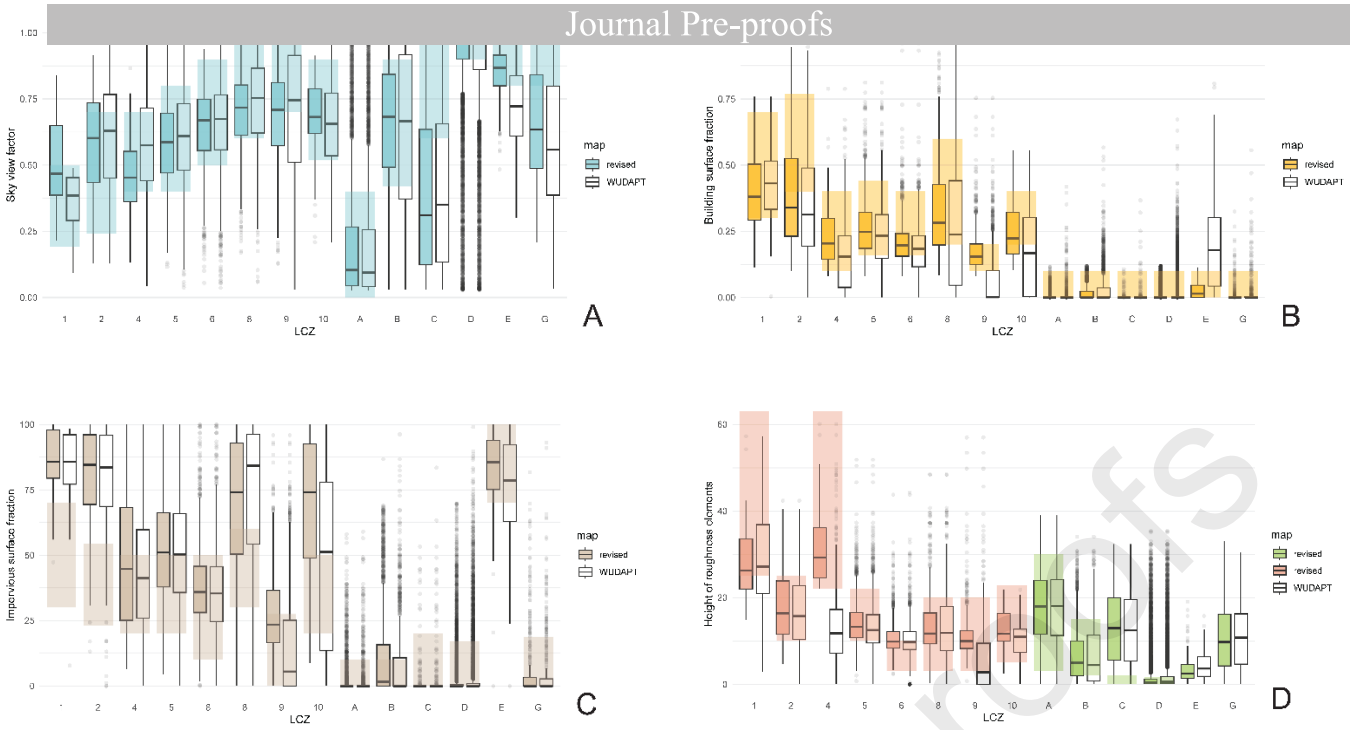

Figure 87: Boxplots of UCP distributions per LCZ class. A) Sky view factor, B) Building surface fraction, C) Impervious surface fraction, and D) Height of roughness elements. Revised map: boxplots with color filling. WUDAPT MAP: boxplots without filling. Bern-specific UCP value ranges: colored rectangles

4 Discussion

The intercomparison and evaluation of the resulting reclassification require a critical discussion regarding the influence of UCP geodata and the adjustment of UCP value ranges, the accuracy of the revised classification, and the usability of the resulting LCZ map.

4.1 UCP geodata as a basis for LCZ revision and evaluation

In general, UCPs are a suitable basis for generating and evaluating LCZ maps. This is also concluded by various studies that have generated GIS-based LCZ maps using UCPs (Hidalgo et al., 2019; Huang et al., 2023; Quan & Bansal, 2021). So far, the combination of GIS and RS-based mapping has only been explored in a few studies (Fonte et al., 2019; Gál et al., 2015; Zhou et al., 2020). UCPs are precisely those characteristics of an urban environment that the LCZ framework summarizes into one single value - the LCZ class. Thus, given that the UCPs are calculated accurately, we can assume that an LCZ is correctly classified if the UCP values match the defined UCP value ranges (Huang et al., 2023). Building upon this premise, our study hypothesized that integrating UCPs as additional input for identifying and correcting misclassifications enhances accuracy. Our results confirm this hypothesis, with an improvement of 9% of an RS-based LCZ classification (WUDAPT workflow) using UCPs.

It is important to differentiate the exact usage of the UCPs among the steps of the revision and evaluation process, namely the misclassifications, reclassification of pixels, and evaluation of the new map. The identification of misclassifications (revision step 1, see Fig. 3) and reclassifications (occurring directly in step 1 and via the decision tree in step 2, see Fig. 3) are inherently linked to the WUDAPT map. In other words, whether a pixel is checked for misclassification and subsequently reclassified depends on the LCZ assigned in the original classification, since only the LCZ classes concerned by the selected misclassification patterns are checked. The Bern-specific UCP value ranges are essential for the result, as they serve as thresholds for the reclassification via decision tree. The KNN algorithm (revision step 3, see Fig. 3) is a new bottom-up classification, relying on mean UCP values rather than thresholds, but also depending on the identification of misclassification and preselected according to a BSF threshold.

The choice of UCP datasets determines the ability to identify misclassifications and, subsequently, to reclassify the concerned pixels. Data availability can be a limiting factor in retrieving UCPs (Aslam & Rana, 2022b; Quan & Bansal, 2021). In Switzerland, various high-quality cadastral data and remote sensing products are available, but this may differ for other study areas. The abundance of data allowed us to retrieve most geometric and surface cover UCPs, except for *aspect ratio*. Thermal UCPs were

not included in the analysis but could, however, be helpful in further characterizing industrial areas and compactly built areas (Qua

Cadastral data allowed us to introduce and retrieve three additional surface fractions (WSF, SSF, and FSF), simplifying the identification and classification of certain land cover LCZs via the decision tree. Since these additional UCPs have yet to be formally agreed upon, comparability to other LCZ maps is limited and there is a risk of introducing biases and errors (Quan & Bansal, 2021). Consequently, their value ranges were set with regard to other studies (Hidalgo et al., 2019; Quan & Bansal, 2021) and through visual crosschecking with aerial images. The effectiveness of the decision tree relies partly on these additional UCPs. For instance, LCZ G could be determined easily by considering the WSF, while LCZ A could be classified based on the FSF alone. In these cases, only one UCP was necessary to delineate the respective LCZ. Only using the UCPs defined by Stewart & Oke (2012) would have made the delineation much more challenging.

The hierarchy by which the UCPs are considered when identifying misclassified pixels via the queries (Tab. 3) and reclassifying them via the decision tree (see Fig. 3 and 4) also plays a role. In this aspect, the presented approach is oriented toward similar studies (Geletič & Lehnert, 2016; Hidalgo et al., 2019). Prioritizing the BSF allows us to reliably distinguish built type from land cover LCZ classes, which solves one of the main issues of inaccuracy. Next in the hierarchy, the data is sorted by degree of soil sealing and further checked for WSF, FSF, and SVF to discriminate among LCZ G and different vegetation cover classes. In the queries, built-up LCZ classes are further categorized using the BH. As an alternative to a complex decision tree, the KNN algorithm was chosen to classify unclassified built-up LCZ pixels with minimal preprocessing. However, due to the limited inclusion of only four UCPs in the training data, the classification lacks important input data to reliably classify all built type LCZs. Proximity between certain training data points and anomalies in UCPs can lead to misclassifications. To address this, potential extensions of the workflow include weighting specific UCPs for certain LCZs (Demuzere et al., 2019), implementing a multi-step classification strategy based on criteria such as building height and impervious surface fraction (Hidalgo et al., 2019) or considering the surrounding LCZs in the classification decision.

4.2 Accuracy of the classification

The revised LCZ map improves the representation of LCZs in Bern, with an 9% increase in overall accuracy to 53%. This is consistent with the accuracies of WUDAPT-generated LCZ maps (Bechtel et al., 2019), although applying a slightly different evaluation approach. The increase is especially valuable since the improvements mainly occurred in the LCZ classes that were focused on, and thus, the most influential misclassifications were tackled. Important small-scale structures like the river, forest patches, green squares, sealed squares, and highways are added or represented more accurately. Errors in building height recognition are corrected, and non-built-up areas are neatly distinct from built-up areas. Notably, a substantial portion (82%) of the WUDAPT map is kept, meaning that our workflow primarily serves to enhance details of the already high-quality WUDAPT workflow.

While the overall accuracy of 53% may not appear particularly high, it is essential to consider the strict criterion of conforming to all tested UCP values for correctly classified pixels. This suggests that the proportion of correctly classified pixels is likely higher, as our rule lacks buffer, tolerance, or weighting. Other studies (Demuzere et al., 2019; Hidalgo et al., 2019) similarly concluded that UCP values of correctly classified LCZs do not fall within established value ranges in a substantial number of cases. Furthermore, the severity of misclassifications can be contextualized to some extent by considering the morphological and microclimatic similarity of LCZ classes (Bechtel et al., 2019). In other words, if a misclassified LCZ differs only slightly from the correct LCZ, the misclassification holds lesser significance. This is only tested for the reclassifications. For morphological similarity, we found that changes appear primarily in land cover type LCZs misclassified as built type LCZs, so in morphologically different classes. Thermal difference is tested according to temperature measurements in different LCZs in Bern. We found that 15% of the reclassifications happen in thermally significantly different classes. Again, this may not seem like particularly high improvements. However, the reclassifications also reflect the selected main patterns, and thus tackle the most severe misclassifications. a combination of thermal and morphological similarity may be more representative as an accuracy assessment and could be explored in further research.

The size and form of mapping units influence the mapping accuracy and can be broadly categorized into gridded and parcel-based (Huang et al., 2023). As LCZs are rarely square-shaped, a gridded map can face the challenge of mixed pixels containing LCZ borders, which may contribute to the unmatching UCP value ranges. To account for the various forms of LCZs, it is therefore advisable to choose a pixel size that is smaller than the average LCZ (Huang et al., 2023), in our case 78.8 x 78.8 m, even though this is far below the 400 m minimum diameter recommended by Stewart & Oke (2012). On the one hand, the high resolution captures the heterogeneous small structures in Bern more accurately. Even small-scale structures can be relevant for temperature variability; for example, small, vegetated areas in Bern have a cooling effect of about 0.5 K (Burger et al., 2021). On the other hand, the high-resolution poses problems such as single pixel LCZs or the splitting of open-built LCZs into checkerboard-like alternations of land cover and built type LCZ (Figure 5D). Quan & Bansal (2021) refer to this problem as “unnecessary heterogeneity”. It distracts from understanding thermal interactions at an urban scale and does not sufficiently summarize built structures.

4.3 Usability, generalizability, and further development

Our approach focuses on key factors that markedly influence Bern's urban climate, including built-up and sealed areas, water bodies, and building height (Burger et al., 2021). While these factors may vary slightly in other cities, they likely apply to European cities of similar structures and urban planning histories (Wicki & Parlow, 2017). The workflow can be easily adapted or simplified based on a city's needs by targeting specific weak points of the LCZ map. For example, a revision could tackle only water surfaces using WSF, sealed surfaces using ISF or SSF, or focus on correcting specific LCZ classes of compact building style (LCZ 1/2/3) or open building style (LCZ 4/5/6) based on their BH.

Especially in small, heterogeneous European cities, the value ranges may differ substantially from those defined by Stewart & Oke (2012) (Mitraka et al., 2015; Wicki & Parlow, 2017). Adjusting specific UCP value ranges according to the value ranges of the training areas ensures that the city's typical UCP value ranges for each LCZ are respected. This avoids overly strict identification of misclassifications. However, it may also introduce systematic biases and limit comparability. Further research is needed on how and to what magnitude the original framework can be adapted.

The impact of unnecessary heterogeneity on the map's usefulness cannot be generalized, as LCZ maps serve various purposes (Aslam & Rana, 2022). For instance, UCPs derived from (usually WUDAPT generated) LCZ maps are used as input to urban climate models (Brousse et al., 2016; Geletič & Lehnert, 2016; Hammerberg et al., 2018)(Brousse et al., 2016; Geletič & Lehnert, 2016; Hammerberg et al., 2018)(Brousse et al., 2016; Geletič & Lehnert, 2016; Hammerberg et al., 2018), which have shown to be sensitive to high-resolution land use variations and therefore benefit from a high level of detail in the LCZ maps (Brousse et al., 2016). Depending on the resolution of the model, the map however would need to be aggregated. Most commonly, LCZ maps are used to assist urban temperature studies (Aslam & Rana, 2022). In Bern specifically, the LCZ map is used in urban climate studies related to the city's low-cost measurement network (Gubler et al., 2021) to evaluate the model results of UHI intensities (Burger et al., 2022; Hürzeler et al., 2022). For these applications, a higher resolution map of 50 m was calculated by resampling (see Appendix). It captures linear elements such as the Aare River, roads, and railways more accurately but intensifies the challenge of unnecessary heterogeneity. In urban planning, high-resolution LCZ maps can be beneficial to identify small-scale cooling or heating areas, but unnecessary heterogeneity could also render an LCZ map more complex. This is dependent on the city's size and the area of the planned construction projects or heat mitigation strategies.

To counteract unnecessary heterogeneity, further research may consider post-processing. A frequently used method to solve the problem of single pixels is the simplest majority rule, which reclassifies an LCZ pixel surrounded by a certain number of different LCZs (Quan & Bansal, 2021). For open-built LCZ types (LCZs 4-6), clarification is needed regarding the size threshold of green spaces that should no longer be considered part of the open building pattern but mapped separately as land cover type LCZs, and similarly, the size threshold for forest patches, water surfaces, or sealed surfaces to be classified as separate LCZs. Furthermore, a typical step in GIS-based classification methods is to fuse basic spatial units (pixels or polygons) into larger areas (Quan & Bansal, 2021; Unger et al., 2014). This would allow to summarize checker-board-like structures into single LCZs. Alternatively, polygons could be chosen as basic spatial units instead of a pixel grid, as they capture the LCZ boundaries better and avoid mixed pixels (Unger et al., 2014; Yan et al., 2022). Urban block units (Quan & Bansal, 2021) or administrative boundaries (Wicki & Parlow, 2017) could be used for the delimitation. Quan & Bansal (2021) generally point out that LCZ mapping is an iterative process of summarization, whose discourse is still too little distinguished from that of the classification of individual sites.

5 Conclusion

This study aims at combining the RS-based mapping tool "LCZ generator" with GIS-based LCZ mapping to address issues of inaccuracy in LCZ maps of heterogeneously structured cities, specifically regarding small-scale structures that are relevant for local climate. Our proposed workflow includes an accuracy assessment of the RS-based LCZ map of Bern, Switzerland, using urban canopy parameter (UCP) geodata and a subsequent revision of the most dominant patterns of misclassifications. The research is motivated by the need for higher detail and accuracy levels in LCZ maps for urban climate studies and climate adaptation planning. As our approach avoids using complex algorithms and is mainly based on simple threshold checking, it is easily applicable and requires no specialized coding. It is also customizable to other maps' inaccuracy issues and introduces a method to adjust UCP value thresholds to a city's individual values.

The findings demonstrate that including UCP geodata improves the LCZ map's overall accuracy by 9%, resulting in 53% of pixels conforming to all tested UCP value ranges (SVF, BSF, ISF, HRE/WSF). The corrections are rather conservative, with 18% of all pixels corrected while keeping 82% of the already accurate WUDAPT map. The revised LCZ map provides more precise information about built structures and surface covers. It depicts small-scale structures that influence urban temperature behavior, particularly water areas, sealed surfaces, sparsely built areas, and transitions between built and non-built areas. Most improvements were achieved in land cover type LCZs misclassified as built type LCZs.

However, it is important to acknowledge some limitations. The choice of resolution is a trade-off between capturing small-scale stru[Journal Pre-proofs]CZ map. Moreover, adjusting UCP value ranges and introducing additional surface fraction UCPs is not a standardized process, which may introduce biases and limit comparability with other studies. The use of the KNN algorithm for reclassifying built type LCZs is compromised through limited and unweighted input parameters, and exploring alternative methods, such as a decision tree-based stepwise classification, could be beneficial. Further research should address challenges related to pixel size and balancing the consideration of heterogeneous, small-scale structures and sufficient generalization. Additionally, investigating the justification and objectivity of adjusting UCP thresholds according to city-specific values would enhance the reliability and applicability of the classification. A further revision of Bern's current LCZ map could consider postprocessing strategies such as the simplest majority rule and the summarization of pixels.

The implications of this research are threefold: Firstly, it adds to the ongoing research on the combination of RS- and GIS-based approaches in LCZ mapping. This supports the goal of accurate worldwide data on urban form and structure (Stewart & Oke, 2012). Secondly, it supports urban climate research in Bern by providing more accurate data for simulations and evaluations. The improved LCZ map can aid in better understanding and predicting the urban heat island effect and its associated risks. Thirdly, it facilitates the communication of urban climate knowledge and informed decision-making for local urban planning, city administration, transportation departments, energy providers, and other stakeholders involved in climate change adaptation in cities.

CRediT authorship contribution statement

Noémie Wellinger: Conceptualization, Methodology, Software, Validation, Formal analysis, Writing - Original Draft, Writing – review & editing, Visualization **Moritz Gubler**: Conceptualization, Writing - Original Draft, , Writing – review & editing, Supervision, Project administration **Flurina Müller**: Conceptualization, Validation, Resources, Writing - Original Draft **Stefan Brönnimann**: Conceptualization, Writing - Original Draft, Writing – review & editing, Supervision, Funding acquisition.

Declaration of Competing Interest:

The authors declare that they have no known competing financial interests or personal relationships that could have appeared to influence the work reported in this paper.

Declaration of Generative AI and AI assisted technologies in the writing process

During the preparation of this work the author used OpenAI's ChatGPT in order to improve clarity, word choice, and structure in certain paragraphs. After using this tool/service, the authors reviewed and edited the content as needed and take full responsibility for the content of the publication.

Data Availability

Datasets and code related to this article can be found at https://doi.org/10.48620/366, on BORIS, the institutional repository of the University of Bern.

Acknowledgments

We want to thank Moritz Burger from the University of Bern for his help in GIS methodology, the provision of UCP datasets, and for proofreading, and Jürg Franke from the University of Bern for his feedback on the evaluation process.

Funding

European Cooperation in Science and Technology (CA20108, COST Action "FAIRNESS")
Swiss National Science Foundation (213362, Project "URBNET")

The funding sources had no involvement in study design; in the collection, analysis and interpretation of data; in the writing of the report; or in the decision to submit the article for publication.

References

Aslam, A., & Rana, I. A. (2022a). The use of local climate zones in the urban environment: A systematic review of data sources, methods, and themes. In *Urban Climate* (Vol. 42). Elsevier B.V. https://doi.org/10.1016/j.uclim.2022.101120

Aslam, A., & Rana, I. A. (2022b). The use of local climate zones in the urban environment: A systematic review of data sources, methods, and themes. In *Urban Climate* (Vol. 42). Elsevier B.V. https://doi.org/10.1016/j.uclim.2022.101120

Bechtel, B., Alexander, P. J., Beck, C., Böhner, J., Brousse, O., Ching, J., Demuzere, M., Fonte, C., Gál, T., Hidalgo, J., Hoffmann, P., Middel, A., Mills, G., Ren, C., See, L., Sismanidis, P., Verdonck, M. L., Xu, G., & Xu, Y. (2019). Generating WUDAPT Level 0 data – Current status of production and evaluation. *Urban Climate*, *27*, 24–45. https://doi.org/10.1016/j.uclim.2018.10.001

Brousse, O., Martilli, A., Foley, M., Mills, G., & Bechtel, B. (2016). WUDAPT, an efficient land use producing data tool for mesoscale models? Integration of urban LCZ in WRF over Madrid. *Urban Climate*, *17*, 116–134. https://doi.org/10.1016/j.uclim.2016.04.001

Burger, M., Gubler, M., Heinimann, A., & Brönnimann, S. (2021). Modelling the spatial pattern of heatwaves in the city of Bern using a land use regression approach. *Urban Climate*, *38*. https://doi.org/10.1016/j.uclim.2021.100885

Chen, Y., Zheng, B., & Hu, Y. (2020). Mapping local climate zones using arcGIS-based method and exploring land surface temperature characteristics in Chenzhou, China. *Sustainability (Switzerland)*, *12*(7). https://doi.org/10.3390/su12072974

Conrad, O., Bechtel, B., Bock, M., Dietrich, H., Fischer, E., Gerlitz, L., Wehberg, J., Wichmann, V., & Böhner, J. (2015). System for Automated Geoscientific Analyses (SAGA) v. 2.1.4. *Geoscientific Model Development*, *8*(7), 1991–2007. https://doi.org/10.5194/gmd-8-1991-2015

Demuzere, M., Bechtel, B., Middel, A., & Mills, G. (2019). Mapping Europe into local climate zones. *PLoS ONE*, *14*(4). https://doi.org/10.1371/journal.pone.0214474

Demuzere, M., Kittner, J., & Bechtel, B. (2021). LCZ Generator: A Web Application to Create Local Climate Zone Maps. *Frontiers in Environmental Science*, *9*. https://doi.org/10.3389/fenvs.2021.637455

Estacio, I., Babaan, J., Pecson, N. J., Blanco, A. C., Escoto, J. E., & Alcantara, C. K. (2019). GIS-BASED MAPPING of LOCAL CLIMATE ZONES USING FUZZY LOGIC and CELLULAR AUTOMATA. *International Archives of the Photogrammetry, Remote Sensing and Spatial Information Sciences - ISPRS Archives*, *42*(4/W19), 199–206. https://doi.org/10.5194/isprs-archives-XLII-4-W19-199-2019

[data] European Environment Agency (EEA) (2020): Imperviousness Density (IMD) 2018. © European Environment Agency. https://land.copernicus.eu/pan-european/high-resolution-layers/impervious-ness/status-maps/2015

Federal Statistical Office (FSO). (2022). *Statistik CH Städte - Wohnbevölkerung*. https://www.bfs.admin.ch/bfs/de/home.assetdetail.20764838.html

Fonte, C. C., Lopes, P., See, L., & Bechtel, B. (2019). Using OpenStreetMap (OSM) to enhance the classification of local climate zones in the framework of WUDAPT. *Urban Climate*, *28*. https://doi.org/10.1016/j.uclim.2019.100456

Gál, T., Bechtel, B., & Unger, J. (2015). Comparison of two different Local Climate Zone mapping methods. *Int. Conf. Urban Clim.* 342–351.

Geletič, J., & Lehnert, M. (2016). GIS-based delineation of local climate zones: The case of medium-sized Central European cities. *Moravian Geographical Reports*, *24*(3), 2–12. https://doi.org/10.1515/mgr-2016-0012

Geletič, J., Lehnert, M., & Dobrovolný, P. (2016). Modelled spatio-temporal variability of air temperature in an urban climate and its validation: A case study of Brno, Czech Republic. *Hungarian Geographical Bulletin*, *65*(2), 169–180. https://doi.org/10.15201/hungeobull.65.2.7

Ginzler, C., & Hobi, M. L. (2015). Countrywide stereo-image matching for updating digital surface models in the framework of the swiss national forest inventory. *Remote Sensing*, *7*(4), 4343–4370. https://doi.org/10.3390/rs70404343

Gorelick, N., Hancher, M., Dixon, M., Ilyushchenko, S., Thau, D., & Moore, R. (2017). Google Earth Engine: Planetary-scale
Journal Pre-proofs
31

Gubler, M., Christen, A., Remund, J., & Brönnimann, S. (2021). Evaluation and application of a low-cost measurement network to study intra-urban temperature differences during summer 2018 in Bern, Switzerland. *Urban Climate*, *37*. https://doi.org/10.1016/j.uclim.2021.100817

Hammerberg, K., Brousse, O., Martilli, A., & Mahdavi, A. (2018). Implications of employing detailed urban canopy parameters for mesoscale climate modelling: a comparison between WUDAPT and GIS databases over Vienna, Austria. *International Journal of Climatology*, *38*, e1241–e1257. https://doi.org/10.1002/joc.5447

Hidalgo, J., Dumas, G., Masson, V., Petit, G., Bechtel, B., Bocher, E., Foley, M., Schoetter, R., & Mills, G. (2019). Comparison between local climate zones maps derived from administrative datasets and satellite observations. *Urban Climate*, *27*, 64–89. https://doi.org/10.1016/j.uclim.2018.10.004

Huang, F., Jiang, S., Zhan, W., Bechtel, B., Liu, Z., Demuzere, M., Huang, Y., Xu, Y., Ma, L., Xia, W., Quan, J., Jiang, L., Lai, J., Wang, C., Kong, F., Du, H., Miao, S., Chen, Y., & Chen, J. (2023). Mapping local climate zones for cities: A large review. In *Remote Sensing of Environment* (Vol. 292). Elsevier Inc. https://doi.org/10.1016/j.rse.2023.113573

Hürzeler, A., Hollósi, B., Burger, M., Gubler, M., & Brönnimann, S. (2022). Performance analysis of the urban climate model MUKLIMO_3 for three extreme heatwave events in Bern. *City and Environment Interactions*, *16*. https://doi.org/10.1016/j.cacint.2022.100090

IPCC. (2023). *Summary for Policymakers*.

James, G. (Gareth M., Witten, D., Hastie, T., & Tibshirani, R. (2013). *An introduction to statistical learning with applications in R*.

MeteoSwiss. (2021). *Klimanormwerte Bern / Zollikofen, Normperiode 1991-2020*.

Mitraka, Z., Del Frate, F., Chrysoulakis, N., & Gastellu-Etchegorry, J. P. (2015, June 9). Exploiting Earth Observation data products for mapping Local Climate Zones. *2015 Joint Urban Remote Sensing Event, JURSE 2015*. https://doi.org/10.1109/JURSE.2015.7120456

Muhammad, F., Xie, C., Vogel, J., & Afshari, A. (2022). Inference of Local Climate Zones from GIS Data, and Comparison to WUDAPT Classification and Custom-Fit Clusters. *Land*, *11*(5). https://doi.org/10.3390/land11050747

[data] Office for Geoinformation of the Canton of Bern (2021): Amtliche Vermessung Vereinfacht (Version: 23.03.2021). © Office for Geoinformation of the Canton of Bern. https://www.agi.dij.be.ch/de/start/geoportal/geodaten/detail.html?type=geoproduct&code=MOPUBE

Oke, T. R., Mills, G., Christen, A., & Voogt, J. A. (2017). *Urban Climates*.

Quan, S. J., & Bansal, P. (2021). A systematic review of GIS-based local climate zone mapping studies. In *Building and Environment* (Vol. 196). Elsevier Ltd. https://doi.org/10.1016/j.buildenv.2021.107791

Stewart, I. D., & Oke, T. R. (2012). Local climate zones for urban temperature studies. *Bulletin of the American Meteorological Society*, *93*(12), 1879–1900. https://doi.org/10.1175/BAMS-D-11-00019.1

[data] swisstopo (2022): Luftbilder Schweiz. © Federal Office of Topography swisstopo. https://map.geo.admin.ch/

Unger, J., Lelovics, E., & Gál, T. (2014). Local climate zone mapping using GIS methods in Szeged. *Hungarian Geographical Bulletin*, *63*(1), 29–41. https://doi.org/10.15201/hungeobull.63.1.3

Vicedo-Cabrera, A. M., Ragettli, M. S., Schindler, C., & Röösli, M. (2016). Excess mortality during the warm summer of 2015 in Switzerland. *Swiss Medical Weekly*, *146*, w14379. https://doi.org/10.4414/smw.2016.14379

Wang, R., Ren, C., Xu, Y., Lau, K. K. L., & Shi, Y. (2018). Mapping the local climate zones of urban areas by GIS-based and WUDAPT methods: A case study of Hong Kong. *Urban Climate*, *24*, 567–576. https://doi.org/10.1016/j.uclim.2017.10.001

Wicki, A., & Parlow, E. (2017). Attribution of local climate zones using a multitemporal land use/land cover classification scheme. *Journal of Applied Remote Sensing*, *11*(2), 026001. https://doi.org/10.1117/1.jrs.11.026001

Yan, Z., Ma, J., He, W., Zhou, J., Lu, H., Liu, G., & Huang, G. (2022). Comparing Object-Based and Pixel-Based Methods for Local

Zhou, X., Okaze, T., Ren, C., Cai, M., Ishida, Y., & Mochida, A. (2020). Mapping local climate zones for a Japanese large city by an extended workflow of WUDAPT Level 0 method. *Urban Climate*, *33*. https://doi.org/10.1016/j.uclim.2020.100660

Appendix A

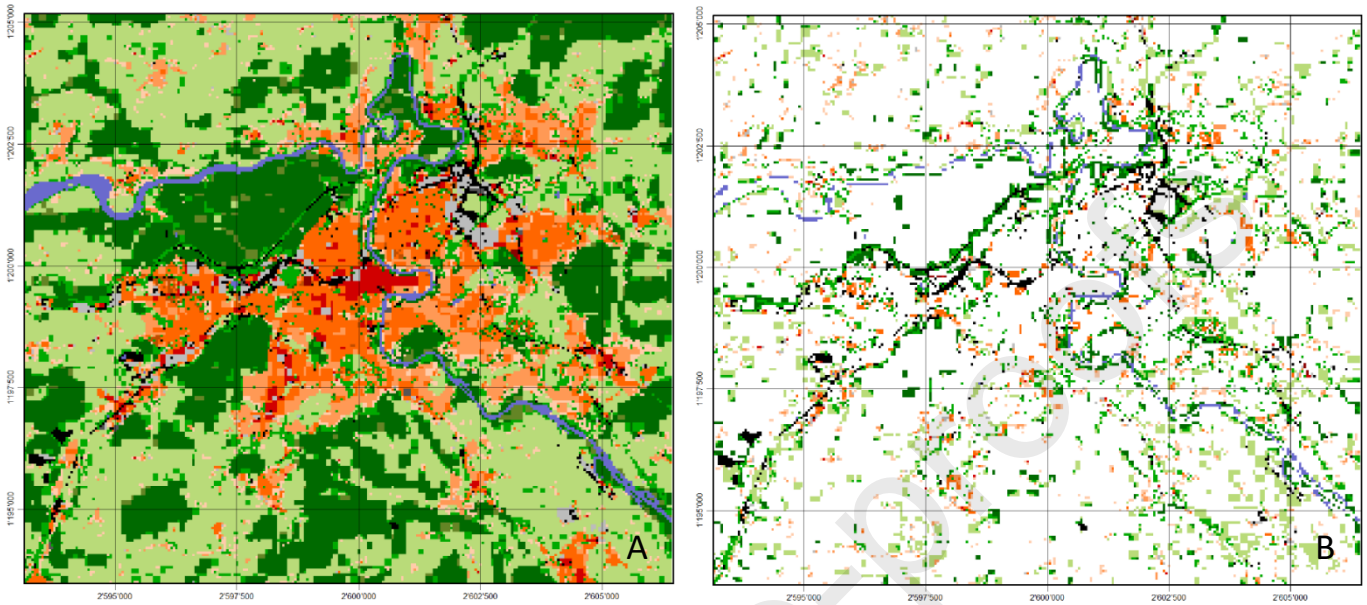

Figure A1: A) Revised LCZ map in 50 m resolution, and B) all pixels that were changed in the revision process.

The station classification of the 80 stations of the urban climate measurement network in Bern (Gubler et al., 2021) is also compared to the mapped LCZs before and after the revision. Standard accuracy measures are calculated in an error matrix (Tab. A1 and Tab A2). The WUDAPT map reaches an overall accuracy (OA) of 42.3% and a Kappa coefficient of 0.34. The OA of the revised map increased to 62.8% with a Kappa coefficient of 0.58.

Table A1: Confusion matrix showing the manually classified LCZs of the reference stations and the LCZs classified by the WUDAPT workflow.

		Reference stations												
	LCZ	**1**	**2**	**4**	**5**	**6**	**8**	**9**	**11**	**12**	**14**	**15**	**17**	**UserAcc. (%)**
WUDAPT map	**2**	0	4	0	1	1	2	0	0	0	0	1	0	44.4
	4	0	1	0	0	0	1	0	0	0	0	0	0	0.0
	5	3	3	1	12	3	1	2	0	1	0	4	0	40.0
	6	0	1	0	1	3	0	2	0	1	0	0	0	37.5
	8	0	1	0	0	0	3	0	0	0	1	0	0	60.0

10	0	1	0	0	0	0	0	0	0	0	0	0	0.0
11	0	0	1	0	1	0	0	2	1	0	0	0	40.0
12	0	0	0	0	0	0	0	1	2	0	0	0	66.7
14	0	0	0	0	1	0	1	0	0	4	0	0	66.7
15	0	0	0	1	0	0	0	0	0	0	0	0	0.0
17	0	0	0	0	0	0	0	0	0	0	0	2	100.0
ProdAcc. (%)	0.0	36.4	0.0	80.0	25.0	42.9	16.7	66.7	40.0	66.7	0.0	66.7	

OA(%)	**42.3**
Kappa	**0.34**

1

2 *Table A2: Confusion matrix showing the manually classified LCZs of the reference stations and the LCZs classified by the revision workflow.*

		Reference stations												
	LCZ	**1**	**2**	**4**	**5**	**6**	**8**	**9**	**11**	**12**	**14**	**15**	**17**	**UserAcc. (%)**
Revised map	**2**	0	8	0	2	0	0	0	0	0	0	2	0	66.7
	4	1	1	1	0	0	0	0	0	0	0	0	0	33.3
	5	1	2	0	13	5	1	1	0	0	0	0	1	54.2
	6	0	0	0	0	6	0	0	0	0	0	0	0	100
	8	1	0	0	0	0	5	0	0	0	0	1	0	71.4
	11	0	0	0	0	0	0	0	3	0	0	0	0	100
	12	0	0	1	0	1	0	1	0	4	1	0	0	50

14	0	0	0	0	0	0	3	0	1	5	0	0	55.6
15	0	0	0	0	0	1	0	0	0	0	2	0	66.7
17	0	0	0	0	0	0	0	0	0	0	0	2	100
ProdAcc. (%)	0.0	72.7	50.0	86.7	50.0	71.4	0.0	100.0	80.0	83.3	40.0	66.7	

OA(%)	**62.8**
Kappa	**0.58**

1

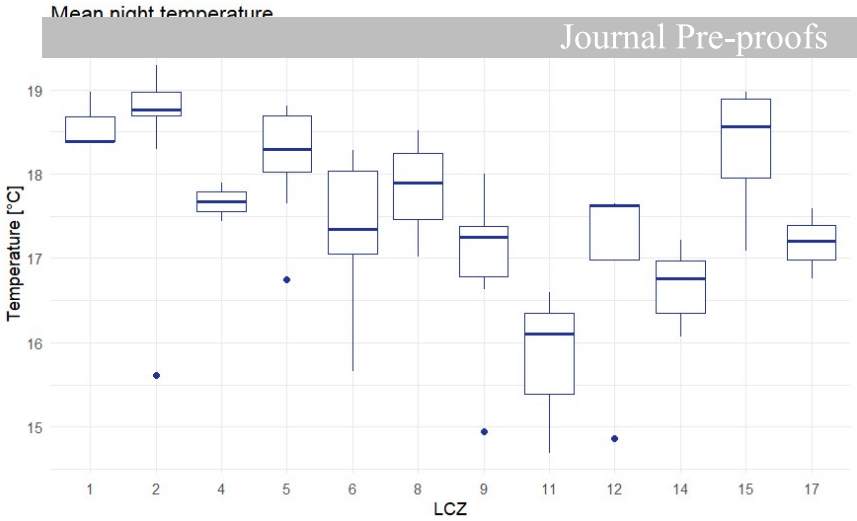

Figure A2: Boxplots showing distribution of mean nighttime temperatures during the summer 2023 (June-August) at the stations of the urban climate network (Gubler et al., 2021)

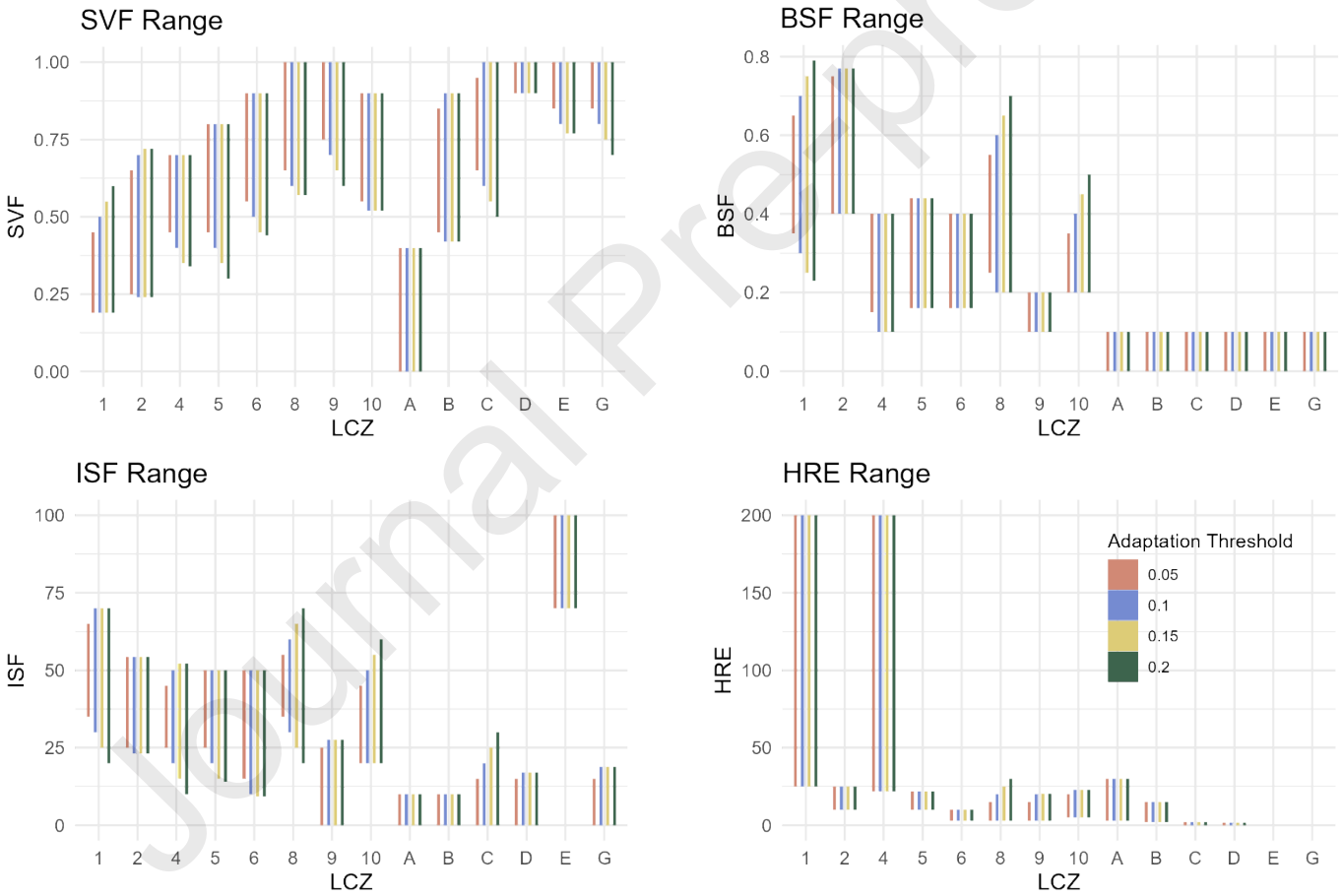

Figure A2: UCP value ranges adapted based on the training area values of Bern's respective LCZ classes. The adapted value ranges are shown for different adaptation thresholds

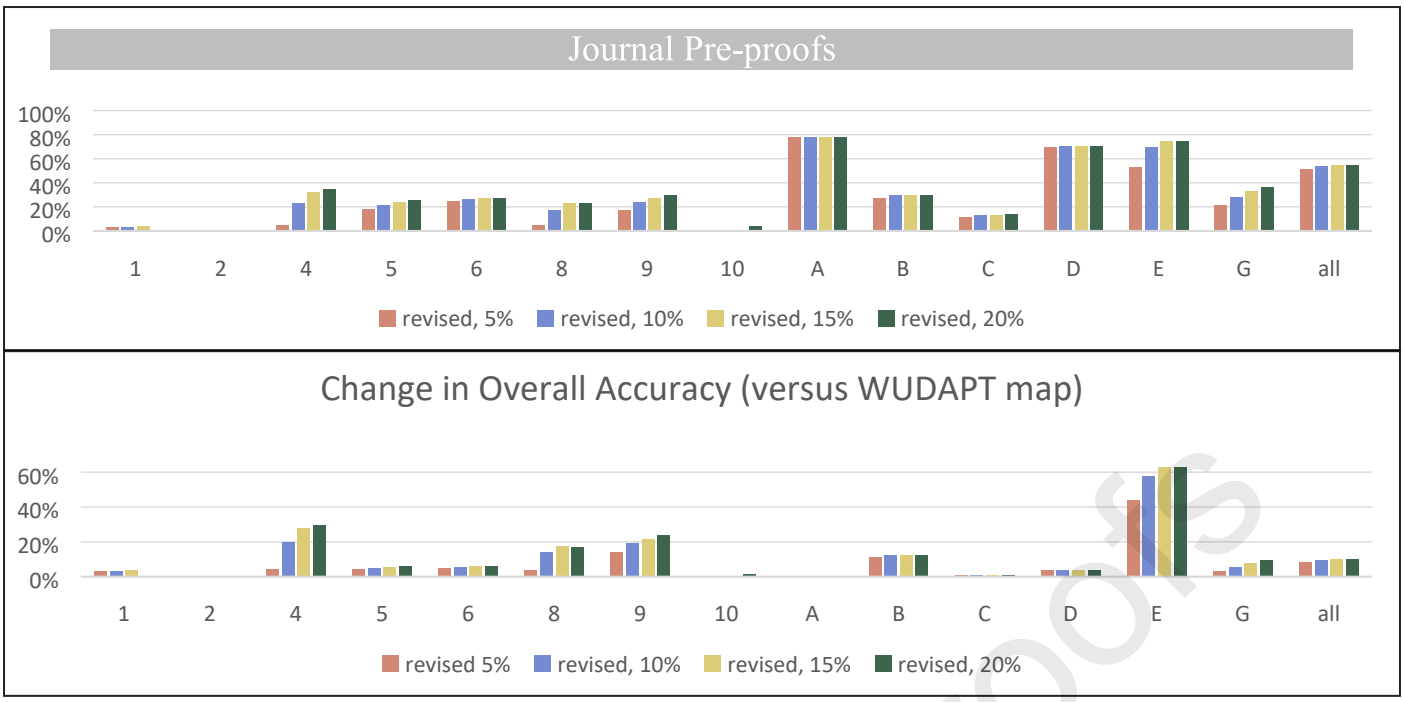

Figure A3: A) Overall Accuracy (OA) for different adaptation thresholds and B) changes in OA for different adaptation thresholds compared to a revision using the standard UCP ranges by Stewart & Oke (2012)

As explained in chapter 2.4, a sensitivity analysis was conducted to measure the influence of the degree of adaptation of the original UCP value ranges by Stewart & Oke (2012). The mean, the standard deviation, as well as the minimum and maximum value of each UCP are calculated for the training areas of each LCZ class. A confidence interval of +/- 2 standard deviations is defined and compared to the established value ranges, which are adjusted if the confidence interval exceeds them. To avoid too severe adaptations, a maximum adaptation threshold should be defined. We conducted a sensitivity analysis, adapting the UCP thresholds by 5%, 10%, 15%, and 20% (Figure A2). We then did the same accuracy assessments as presented in chapter 3.4. We found that the thresholds only marginally influence the overall accuracy, with an OA of 51% for a threshold of 5%, 53% OA for 10%, 54% OA for 15%, and 55% for 20% (Figure A3A). Looking at the individual classes, especially the built type LCZs, as well as LCZ E and G are more accurate, the higher the threshold is set. But since these LCZs make up a small portion of the entire map (LCZ A and D together for example, make up almost 60% of all pixels and their accuracy is not influenced by the thresholds), it does not influence the OA much (Figure A3A).

On the one hand, since a good portion of the UCP minimum and maximum values are not explicitly used in the revision, adapting them will have no impact on the results. On the other hand, some of UCP values used in the revision are set manually or blocked from adaptation, like explained in chapter 2.4. Therefore, they are not affected by the threshold for the adjustment. This can be seen, for example, in the minimum ISF of LCZ E, which is set to 70% or on the HRE ranges of LCZs 1-6 which are blocked from adaptation, since they are such defining parameters.

Since there is not much research yet about adapting UCPs for individual cities, we refrain from adapting the UCPs too much and decided to use the threshold of 10% because it seems to be a good compromise between the original framework and a more intense adaptation and ensures that the UCP ranges do not overlap too much.

Declaration of interests

☐ The authors declare that they have no known competing financial interests or personal relationships that could have appeared to influence the work reported in this paper.

☒ The authors declare the following financial interests/personal relationships which may be considered as potential competing interests:

Prof. Dr. Stefan Broennimann reports financial support was provided by European Cooperation in Science and Technology. Prof. Dr. Stefan Broennimann reports financial support was provided by Swiss National Science Foundation.